ALVEY VISION CONFERENCE, pp. 129-135, MANCHESTER, ENGLAND, SEPTEMBER 1988

Improved Local Flow

Shaogang Gong *

Robotics Research Group
Department of Engineering Science
University of Oxford

In order to understand the parallel computation of optic flow, we introduce here a novel algorithm for computing the flow field at certain locations in the image. These locations are on the gradient edges, which Brady calls seeds [1] . *Our Curve Motion Constraint Equation provides an additional constraint to fully and locally estimate the flow field at seeds. Our initial computational experiments have used the improved local flow as the initial input to Hildreth's algorithm. Now we are exploring an algorithm to perform the whole computation in parallel.*

1 Introduction

Horn and Schunck's motion constraint equation provides one constraint on the optic flow vector at any position in an image. This raises the "aperture problem" in the two-dimensional apparent motion computation. In order to fully constrain or estimate the optic flow, they assumed that the physical world is locally smooth everywhere, as is the three-dimensional motion field. As optical projection preserves smoothness into the two-dimensional motion field, and also because of the similarity between the two-dimensional motion field and the two--dimensional optic flow, the optic flow is locally smooth everywhere in the image. By using the smoothness assumption to regularise the flow field (to achieve global minimisation), they suggested that the aperture problem can be overcome [6]. Under egomotions in which the camera moves against a static environment, the motion field does seem to be smooth, as does the optic flow. But the flow field in a general situation which contains at least one moving object against a static background, will not be smooth. Also, depth discontinuities give rise to the motion field discontinuities [15], [3], [2], [16]. Instead of smoothing the flow field in two-dimensions, Hildreth's scheme only smooths the flow along one-dimensional curves corresponding to the zero crossings of the image. The arguments for doing so are based on: physiological evidence [5], the numerical conditioning of the motion constraint equation and, the physical adequacy for assuming smoothness along edges rather than everywhere in the image. Hildreth's approach is supported by some experimental results [5], [3]. Though it is clearly one of the best schemes proposed for estimating optic flow (at least along curves), it is inherently sequential [3]. Alternatively, Scott's Four Line Method [15] computes a dense optic flow similar to that of Horn and Schunck, but he argues that the flow field across a motion boundary won't be smoothed out, and furthermore, the match procedure used in the scheme is local instead of a global regularisation, which overcomes the sequential computation problem associated with Hildreth's scheme. In practice, the match scheme employed in Scott's algorithm tends to propagate the flow field into the static background region which has any local edge structure. This gives the effect of a "wake" surrounding moving objects, though it employs some novel ideas which combines different smoothness assumptions according to the different intensity structures into a single scheme [3].

Imposing observational assumptions, such as smoothness, about the physical world, are aimed to overcome the aperture problem by introducing another constraint. Most people simply apply regularisation to achieve a global minimisation. There are hardly ideas about trying to find a local constraint which can fully estimate the optic flow only applying local computation. Koenderinck has carried out some theoretical investigations from biological point of view [8], [7]. Theoretically as well as practically, we have been inspired by Nagel's work [10], [9], [11].

The work represented in this paper is to understand the degree of constraint on the optic flow computation at the seed locations as we will describe later [1]. We claim that at the seed locations, we can fully estimate the optic flow locally. Similar work has been carried out by Nagel in his second order Taylor series expansion of the intensity function. Nagel showed that at "grey value corners", the full flow can be computed by his second order equation [10]. More recently, Nagel shows that employing the smoothness assumption along the edges as Hildreth does, or other kinds of 'oriented smoothness' assumptions are implicitly employing the higher order of Taylor expansion of the intensity function [11]. But, Nagel's method concerns how to compute the flow field in a two--dimensional local region. As we said before, in general, there are flow discontinuities across the image, we believe that trying to estimate the two-dimensional flow field before knowing the boundaries of the flow discontinuity will risk the danger to cross these boundaries in the computation. This will blur the flow across the different objects which carry on different motions. Therefore, we attempt to understand here the local constraint at the locations *along* the edges.

2 Seeds and its constraints

The *Seeds* are locations of two-dimensional constraint [1], examples of which include Nagel's "grey value corners", or other kinds of models based on the change of second order derivatives of the intensity function [4], [12], etc. At seed locations, we have a two-dimensional constraint on the flow vector which means that in theory, we can fully estimate the two--dimensional flow locally. This observation has been noted previously [9], [11], [1], etc.

Instead of trying to recover the optic flow field everywhere in the image by a single mechanism, we believe that there

*The author acknowledges the support of the Royal Society and GEC Hirst Research Laboratories.

are different schemes for estimating the flow associated with different intensity structures. In the image, there are loci that offer differing constraints, namely points within regions of smooth change or constant intensity value, points of one--dimensional intensity discontinuity which are often associated with image edges, and points of two-dimensional discontinuity of the intensity which are seeds, are distinguish. Furthermore, according to the degree of the constraint, there are degrees of locality. This means when the constraint is decreases, the associated condition for locally estimating the full flow also decreases. There are loci in the image at which we can completely and locally compute the flow without global assumptions. But, as the constraint decreases, we need a different schemes for estimating the flow in those less constrained locations which can not be done locally. Therefore, the parallel computation of two-dimensional apparent motion can not be employed throughout all stages of the computation. This suggests that the computation of the optic flow is a multiple level mechanism in the sense that different levels are associated with a certain degree of well-conditioning as well as of parallelism. The question of parallel computation of visual motion is to maximally employ the degree of parallelism, which are different in different stages of the computation, rather than trying to employ a single parallel computation mechanism all the way through the motion estimation. Similar suggestions are to be found in physiological and psychological experiments [13], [14].

3 Mathematical structure of the edge flow

We study the conditions in which we can locally compute both components of the optic flow (full flow) along an edge.

We start from the *motion constraint equation* (m.c.e):

$$\nabla \mathbf{I} \cdot \mu + I_t = 0 \tag{1}$$

which derives from an assumption of temporally constant intensity. $\nabla \mathbf{I}$ is the first order spatial gradient vector, μ is the optic flow vector, which is defined as:

$$\mu = \left[\begin{array}{cc} dx/dt & dy/dt \end{array} \right]^{\top}, \tag{2}$$

and I_t is the temporal gradient at a pixel. The relationship between the spatial and temporal gradients and the optic flow vector is then:

$$\mathbf{N} \cdot \mu = -\frac{I_t}{\|\nabla I\|} \tag{3}$$

where $\mathbf{N} = \nabla \mathbf{I}/\|\nabla I\|$ is the unit vector in the direction of the intensity gradient.

As we said before, equation 3 imposes one local constraint on the two-dimensional optic flow vector. If the norm of spatial gradient $\|\nabla I\|$ is small, this computation will be poorly--conditioned. This is the numerical argument in favour of edge motion estimation. Therefore, we restrict our attention to those image loci which have high first-order spatial gradient, edges ($\nabla^2 \mathbf{I}$). At such an edge point, an *edgel*, the intensity gradient is orthogonal (in the image plane) to the (tangent to the) edge.

To understand the mathematical structure of the flow field along an edge, we examine an edge in a temporal sequence of images. In one representation, edgels are addressed by their image coordinates (x, y); and in another representation, the same point is accessed by its distance s along the edge. Adding the time parameter t, we denote the quantities that feature in our analysis as follows:

$I(x, y, t)$:	intensity at a point in the image.
$I(s, t)$:	intensity of an edgel.
$\gamma(s, t)$:	an edge.
$x(s, t)$:	x coordinate of a point on the edge.
$y(s, t)$:	y coordinate of a point on the edge.
$\nabla \mathbf{I}$:	spatial gradient of a pixel.
$\mathbf{N}$:	unit vector in the gradient direction.
$\mathbf{T}$:	unit vector orthogonal to $\mathbf{N}$.
μ :	velocity vector of a pixel.
$\mathbf{H}$:	Hessian matrix of a pixel.

The position along an edge is given by s, at any instant time t_i, and at any particular point on the edge, we have:

$$\mathbf{T} = \frac{\partial \gamma}{\partial s}|_{t=t_i} \quad where \quad \gamma = \gamma(s, t)$$

In other words:

$$\mathbf{T} = \left[\begin{array}{cc} \partial x/\partial s & \partial y/\partial s \end{array} \right]^{\top} \tag{4}$$

After these statements have been cleared, it can be shown what the tangential component of the flow vector along an edge should be. First we have the Taylor expansion of the optic flow along an edge, which is:

$$\mu(s + \Delta s) = \mu(s) + \frac{\partial \mu}{\partial s}\Delta s + \frac{\partial^2 \mu}{\partial s^2}\Delta s^2 + O(\Delta s^3)$$

Similarly, the Taylor expansion of $\nabla \mathbf{I}$ and I_t along an edge should be:

$$\nabla \mathbf{I}(s + \Delta s) = \nabla \mathbf{I}(s) + \frac{\partial \nabla \mathbf{I}}{\partial s}\Delta s + \frac{\partial^2 \nabla \mathbf{I}}{\partial s^2}\Delta s^2 + O(\Delta s^3)$$

$$I_t(s + \Delta s) = I_t(s) + \frac{\partial I_t}{\partial s}\Delta s + \frac{\partial^2 I_t}{\partial s^2}\Delta s^2 + O(\Delta s^3)$$

Ignore the triple and higher order of Δs in the above equations, we have:

$$\mu(s + \Delta s) = \mu(s) + \frac{\partial \mu}{\partial s}\Delta s + \frac{\partial^2 \mu}{\partial s^2}\Delta s^2 \tag{5}$$

$$\nabla \mathbf{I}(s + \Delta s) = \nabla \mathbf{I}(s) + \frac{\partial \nabla \mathbf{I}}{\partial s}\Delta s + \frac{\partial^2 \nabla \mathbf{I}}{\partial s^2}\Delta s^2 \tag{6}$$

$$I_t(s + \Delta s) = I_t(s) + \frac{\partial I_t}{\partial s}\Delta s + \frac{\partial^2 I_t}{\partial s^2}\Delta s^2 \tag{7}$$

Now, consider the motion constraint equation in the neighbourhood of a point at distance s along the edge, which is:

$$\nabla \mathbf{I}(s + \Delta s) \cdot \mu(s + \Delta s) + I_t(s + \Delta s) = 0 \tag{8}$$

Substitute equations 5, 6 and 7 into this neighbourhood m.c.e; then, ignoring the triple and higher order of Δs gives:

$$\begin{aligned} &(\nabla \mathbf{I} \cdot \mu + I_t) + (\nabla \mathbf{I} \cdot \frac{\partial \mu}{\partial s} + \frac{\partial \nabla \mathbf{I}}{\partial s} \cdot \mu + \frac{\partial I_t}{\partial s})\Delta s \\ &+(\frac{\partial \nabla \mathbf{I}}{\partial s} \cdot \frac{\partial \mu}{\partial s} + \mu \frac{\partial^2 \nabla \mathbf{I}}{\partial s^2} + \nabla \mathbf{I} \cdot \frac{\partial^2 \mu}{\partial s^2} + \frac{\partial^2 I_t}{\partial s^2})(\Delta s)^2 \quad = \quad 0 \end{aligned}$$

The partial derivatives of intensity and velocity with respect to a spatial coordinate in two-dimensions are constant. Therefore, in order to satisfy this equation, the coefficients of zero, first and second order in Δs should respectively be 0. This leads to:

$$\nabla \mathbf{I} \cdot \mu + I_t = 0 \tag{9}$$

$$\nabla \mathbf{I} \cdot \frac{\partial \mu}{\partial s} + \frac{\partial \nabla \mathbf{I}}{\partial s} \cdot \mu + \frac{\partial I_t}{\partial s} = 0 \qquad (10)$$

$$\frac{\partial \nabla \mathbf{I}}{\partial s} \cdot \frac{\partial \mu}{\partial s} = 0 \qquad (11)$$

Equation 9 is the motion constraint equation. Equations 10 and 11 provide two new relationships between the intensity and the flow along an edge. What do equations 10 and 11 tell us ? After some mathematical manipulations on the first order equation 10, we derive the following:

$$(\mathbf{T}^\top \mathbf{H}\mathbf{N})(\mathbf{N} \cdot \mu) + (\mathbf{T}^\top \mathbf{H}\mathbf{T})(\mathbf{T} \cdot \mu) - (\mathbf{T}^\top \mathbf{H}\mu) = 0 \qquad (12)$$

Similarly, from the second order equation 11, we obtain:

$$(\mathbf{T}^\top \mathbf{H}\mathbf{N})\{(\mathbf{T}^\top \mathbf{H}\mu) + (\nabla \mathbf{I_t} \cdot \mathbf{T})\} = 0 \qquad (13)$$

where $\nabla \mathbf{I_t}$ is the temporal gradient of the spatial gradient. Clearly, equation 12 provides no additional information. However, equation 13 links the tangential and normal components of the optic flow along the edge. This will be seen in more detail from the following.

From equation 13, we have either:

$$\mathbf{T}^\top \mathbf{H}\mathbf{N} = 0 \quad or \quad (\mathbf{T}^\top \mathbf{H}\mu) + (\nabla \mathbf{I_t} \cdot \mathbf{T}) = 0$$

If $(\mathbf{T}^\top \mathbf{H}\mathbf{N})$ is zero, then either $\mathbf{H}\mathbf{T}$ is parallel to $\mathbf{T}$ or, it is 0. Now:

$$\begin{aligned} \frac{\partial \nabla \mathbf{I}}{\partial s} &= \frac{\partial \|\nabla I\|}{\partial s}\mathbf{N} + \|\nabla I\| \frac{\partial \mathbf{N}}{\partial s} \\ &= (\mathbf{T}^\top \mathbf{H}\mathbf{N})\mathbf{N} + (\mathbf{T}^\top \mathbf{H}\mathbf{T})\mathbf{T} = \mathbf{H}\mathbf{T} \end{aligned}$$

and so *in general*, $(\mathbf{H}\mathbf{T})$ is not parallel to $\mathbf{T}$, nor is it equal to $\mathbf{0}$. In other words, generally we have the *Curve Motion Constraint Equation* (c.m.c.e) as following:

$$(\mathbf{T}^\top \mathbf{H}\mathbf{N})(\mathbf{N} \cdot \mu) + (\mathbf{T}^\top \mathbf{H}\mathbf{T})(\mathbf{T} \cdot \mu) = -(\nabla \mathbf{I_t} \cdot \mathbf{T}) \qquad (14)$$

Is there any special case for which $\mathbf{T}^\top \mathbf{H}\mathbf{N}$ vanishes? As:

$$(\mathbf{T}^\top \mathbf{H}\mathbf{N})\mathbf{N} + (\mathbf{T}^\top \mathbf{H}\mathbf{T})\mathbf{T} = \mathbf{H}\mathbf{T}$$

which means if,

$$\mathbf{T}^\top \mathbf{H}\mathbf{N} = 0 \quad \Rightarrow \quad \mathbf{H}\mathbf{T} = (\mathbf{T}^\top \mathbf{H}\mathbf{T})\mathbf{T}$$

As we have:

$$\kappa = -\frac{1}{\|\nabla I\|}(\mathbf{T}^\top \mathbf{H}\mathbf{T})$$

which κ is the curvature of the edge, therefore:

$$\mathbf{H}\mathbf{T} = -\kappa \|\nabla I\| \mathbf{T}$$

If $\mathbf{H}\mathbf{T}$ is parallel to $\mathbf{T}$, $\mathbf{T}^\top \mathbf{H}\mathbf{N}$ equals to 0. In fact, we found analytically that this situation happens along a circular edge. This may explain why we can not compute a circular object's rotation about its centre, for which all the full flow vectors on the edge only have tangential component.

Except for the case that $\mathbf{H}\mathbf{T}$ is parallel to $\mathbf{T}$, furthermore, being 0 — in other words, edge is a straight line, also makes $\mathbf{T}^\top \mathbf{H}\mathbf{N}$ vanishing. This gives:

$$\mathbf{0} = \begin{bmatrix} \partial I_x/\partial s & \partial I_y/\partial s \end{bmatrix}^\top = \mathbf{H}\mathbf{T} \qquad (15)$$

It says that both $\partial I_x/\partial s$ and $\partial I_y/\partial s$ are equal to zero, which gives the following:

1. At first, equation 15 can be more explicitly written as:

$$\mathbf{0} = \mathbf{H}\mathbf{T} = \frac{1}{\|\nabla I\|} \begin{bmatrix} I_{xx}I_y - I_{xy}I_x \\ I_{xy}I_y - I_{yy}I_x \end{bmatrix} \qquad (16)$$

which means:

$$I_{xx}I_y - I_{xy}I_x = 0, \quad I_{xy}I_y - I_{xy}I_x = 0$$

This obviously gives us: $I_{xx}I_{yy} = I_{xy}^2$. Therefore, where the edge is straight, we have:

$$det\mathbf{H} = 0$$

2. Secondly, as:

$$(\mathbf{T}^\top \mathbf{H}\mu) + (\nabla \mathbf{I_t} \cdot \mathbf{T}) = (\nabla \mathbf{I_t} \cdot \mathbf{T}) \neq 0$$

which means where the edge is straight, c.m.c.e doesn't hold.

By this stage, we have determined a relationship between the edge's optic flow and the corresponding intensity structure. This can be briefly summaried as:

conditions if we assume: *in general, the second order derivatives of the intensity function exist locally*, then we have:

1. To require an edge being straight, means that the determinant of the local *Hessian* matrix equals to zero.
2. Theoretically, we can estimate both components of optic flow locally along edges wherever the edge is not straight, though we still can not estimate the circular objects rotating according to its centre. Practically, we need to concern ourselves with the numerical condition of the c.m.c.e. It is very similar to the situation that arises in using the m.c.e. For the m.c.e, it is judged by the norm of the gradient. For the c.m.c.e, it is judged by $det\mathbf{H}$. In fact, $det\mathbf{H} = \kappa_1\kappa_2(EG - F^2)$, in which E, F and G are the components of the first fundamental form [12], which suggested that the intensity surface shape can be basically classified into three types based on the value of $det\mathbf{H}$. That is:

   $det\mathbf{H} < 0$, hyperbolic point;
   $det\mathbf{H} > 0$, elliptic point;
   $det\mathbf{H} = 0$, parabolic point.

   The parabolic points are associated with the straight edges in the intensity surface, but both hyperbolic and elliptic points are associated with seed locations.
3. Furthermore, where the $det\mathbf{H}$ equals to zero, the optic flow estimation reverts to be an under--determined problem.

What can deduce about the c.m.c.e ? First of all, we can write the c.m.c.e. in a more general form as: $\phi(\mathbf{T} \cdot \mu) + \varphi(\mathbf{N} \cdot \mu) + \lambda = 0$. So the equation gives the correct solution in two kinds of extreme situations (figure 1).

Secondly, we see that Hessian matrix plays a central role here. In practice, we only can compute the $\mathbf{T} \cdot \mu$ where $\mathbf{H}$ is well-conditioned. As $\mathbf{H}$ is associated with the surface curvature of the intensity function [17], [10], [12], large Hessian determinant is associated with the loci of local maximum surface

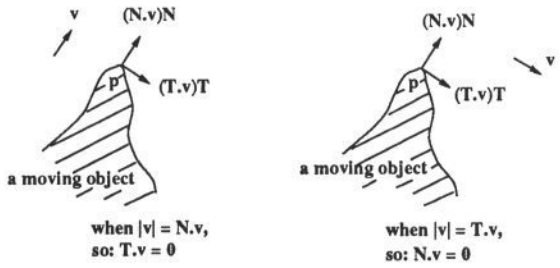

Figure 1: Two extreme situations for the flow flied computation.

curvature on the intensity surface, which are the loci of two--dimensional constraint. Therefore, they correspond to loci of seeds, where we can give a full value for the optic flow. Though it seems to be similar to Nagel's *grey value corners*, we derived here an explicit connection between the structure of intensity on the edge and the constraint for computing the optic flow at these locations. This connection generalises Nagel's method by giving explicit detail about not only dealing with the flow of two-dimensional constraint loci — grey value corners; but also dealing with the flow of one-dimensional constraint loci — edges, and about the degree of numerical reliability for local flow computation on these edges.

4 Improved local flow for edge's flow

Our first application of c.m.c.e is to give an improved local flow as the initial data for Hildreth's scheme. First we give an improved model which is based on the Hildreth's original approach but consider the new local information from the c.m.c.e.

In general, there will be error in both the local computation of $\mathbf{N}\cdot\mu$, which is denoted as $\mu^{\perp}$, and $\mathbf{T}\cdot\mu$ denoted as $\mu^{\top}$. This is caused by image quantisation error and image noise, etc. Therefore, in practice, we require only that the flow obey these local constraints approximately. Combining this approximate requirement with the general smoothness assumption along the edge, we have the following functional to be minimised:

$$\begin{aligned}\Theta &= \int[(\frac{\partial\mu_x}{\partial s})^2+(\frac{\partial\mu_y}{\partial s})^2]ds\\ &+\alpha\int[\mathbf{N}\cdot\mu-\mu^{\perp}]^2ds\\ &+\beta\int[\mathbf{T}\cdot\mu-\mu^{\top}]^2ds \qquad (17)\end{aligned}$$

The parameter α is a weighting factor which expresses the degree of confidence in the local normal flow from the motion constraint equation. β is another weighting factor for the local tangential flow. We set α to be a constant, but set β to be a function of the local Hessian matrix which is varying along the edge.

$$\beta = \frac{det\mathbf{H}}{\epsilon}$$

The function represents two aspects of error sources in the tangential flow computation, where ϵ expresses the degree of confidence in the computation of the Hessian matrix itself, and the determinant of Hessian represents the degree of confidence in using the c.m.c.e. In general, ϵ should be the *condition number* of the Hessian matrix:

$$\epsilon = \|\mathbf{H}\|\|\mathbf{H}^{-1}\|$$

where ϵ equals to 1 corresponding to well-conditioned, and ∞ corresponding to singular. Also, in general, β should be smaller than α, as the error in the computation of second order derivatives are bigger than in the first order derivatives. The discrete function for the first, second and third term in the functional of equation 17 are as follows:

$$\begin{aligned}\Theta_1 &= \sum_{i=2}^{n}[(\mu_{x_i}-\mu_{x_{i-1}})^2+(\mu_{y_i}-\mu_{y_{i-1}})^2]\\ &+[(\mu_{x_1}-\mu_{x_n})^2+(\mu_{y_1}-\mu_{y_n})^2]\end{aligned}$$

$$\Theta_2 = \alpha\sum_{i=1}^{n}[\mu_{x_i}N_{x_i}+\mu_{y_i}N_{y_i}-\mu_i^{\perp}]^2$$

$$\Theta_3 = \frac{det\mathbf{H}}{\epsilon}\sum_{i=1}^{n}[\mu_{x_i}T_{x_i}+\mu_{y_i}T_{y_i}-\mu_i^{\top}]^2$$

From Θ_1, Θ_2 and Θ_3, we have the discrete formula for equation 17 as:

$$\Phi = \Theta_1+\Theta_2+\Theta_3 \qquad (18)$$

Now, the question of minimising equation 17 leads to the question of finding a set of x and y components of the flow, which minimise the discrete function Φ in equation 18. This gives a set of $2n$ linear equations, which are:

$$\frac{\partial\Phi}{\partial\mu_{x_i}}=0,\quad \frac{\partial\Phi}{\partial\mu_{y_i}}=0,\quad 1\le i\le n. \qquad (19)$$

to be solved. This leads to:

$$\begin{aligned}&[4+2\alpha(N_{x_i})^2+2\frac{det\mathbf{H}}{\epsilon}(T_{x_i})^2]\mu_{x_i}-2\mu_{x_{i+1}}\\ &-2\mu_{x_{i-1}}+[2\alpha N_{x_i}N_{y_i}+2\frac{det\mathbf{H}}{\epsilon}T_{x_i}T_{y_i}]\mu_{y_i}\\ &=2\alpha N_{x_i}\mu_i^{\perp}+2\frac{det\mathbf{H}}{\epsilon}T_{x_i}\mu_i^{\top}\\ &1\le i\le n.\end{aligned}$$

and,

$$\begin{aligned}&[4+2\alpha(N_{y_i})^2+2\frac{det\mathbf{H}}{\epsilon}(T_{y_i})^2]\mu_{y_i}-2\mu_{y_{i+1}}\\ &-2\mu_{y_{i-1}}+[2\alpha N_{x_i}N_{y_i}+2\frac{det\mathbf{H}}{\epsilon}T_{x_i}T_{y_i}]\mu_{x_i}\\ &=2\alpha N_{y_i}\mu_i^{\perp}+2\frac{det\mathbf{H}}{\epsilon}T_{y_i}\mu_i^{\top}\\ &1\le i\le n.\end{aligned}$$

These two equations constitute an improved model relative to Hildreth's original scheme [5]. It uses more local information both from m.c.e. and c.m.c.e. to give a faster algorithm.

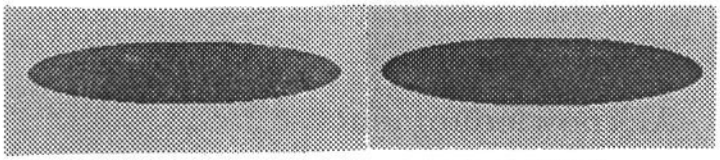

first pixture deforming 2 pixels

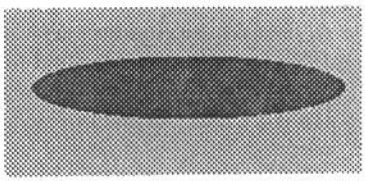

traslation - 2 pixels down

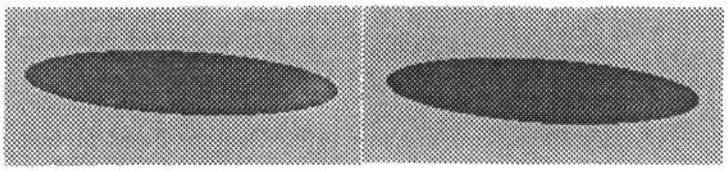

rotation - 3 degrees clockwise general motion

Figure 2: Synthetic image sequences for the experiment of c.m.c.e.

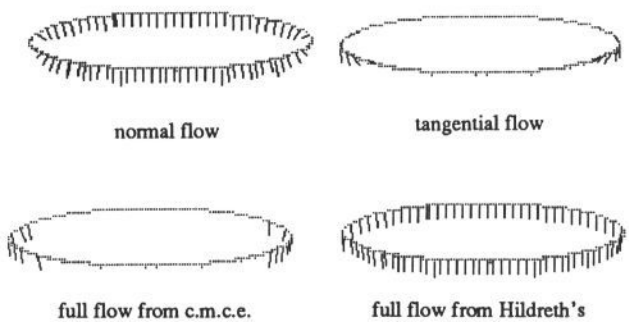

Figure 3: Synthetic translation — 2 pixels down the y direction.

5 Experimental results

In order to show that our model works on practical images, we show the results of some initial experiments. First we give some results which are for testing the c.m.c.e. Secondly, we show some results from our improved version of Hildreth's algorithm.

We first explain the pictures we use here. The aim of this part of the experiment is to show whether the equation works based on the degree of curving on the edges which we have shown theoretically. Therefore, we try to use a kind of image which has less influence from other aspects, such as noise in the image which leads to errors in edge detection and so on. This leads us to use a sequence of synthetic ellipse images which has different curvature along its boundary which is going to give us an edge that can be used for the experiment here. The image sequences include translation, rotation and deformation (see figure 2). The size of images is 128×128.

The resulting flows are shown in figures 3, 4, 5 and 6, which each figure also shows a result from Hildreth's method, but all of them are about fifteen times faster. We note that most time consuming in the computation spends on computing all the derivatives for which we are using relatively large masks (7×7 and 9×9) because the computation of the second order derivatives are very sensitive in general. On the other hand,

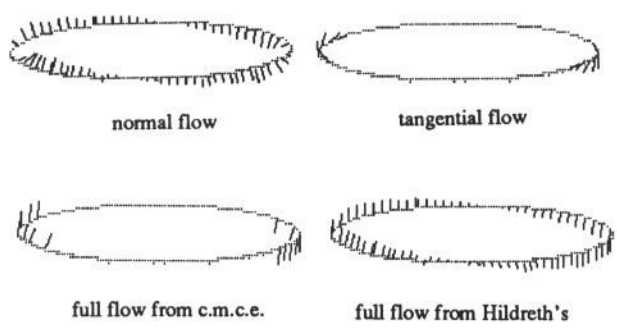

Figure 4: Synthetic rotation — 3° clockwise.

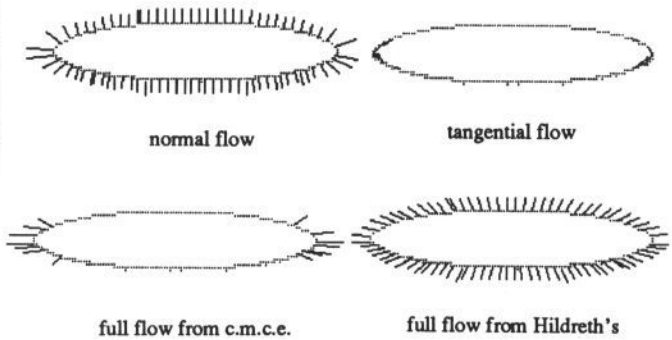

Figure 5: Synthetic deformation — 2 pixels in all directions.

the computing time in Hildreth's method is mostly spent in the iteration stage which is inherently sequential. Therefore we can further speed up the seed motion computation considerably and easily by using a hardware image processing array. In figure 3, we have a translation in which the local normal flow of the loci of seed are useless. The recovered local tangential flow complement the local full flow rather well. This associates with the two extreme situations we mentioned before. Figure 4 and 5 give the results from a rotation (three degrees clockwise). The tangential flow gives a reasonably accurate contribution to the full flow at the seed loci. Finally, figures 5 and 6 show two flows associated with a motion of two pixels deforming in all directions, and a motion of rotation in three degrees clockwise and translation of two pixels in both x and y directions. In these more general situations, the c.m.c.e still gives a quite reasonable local tangential flow.

We have demonstrated the adequacy on sequences of synthetic images. But these are images that have simple structure. For real images, the situation is going to be changed

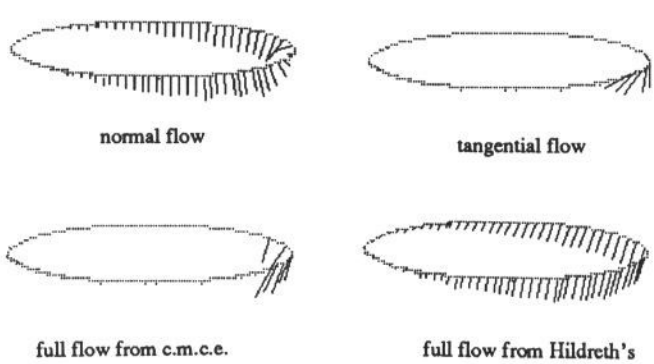

Figure 6: Synthetic general motion — translating 2 pixels in both x and y directions; also rotating 3° clockwise.

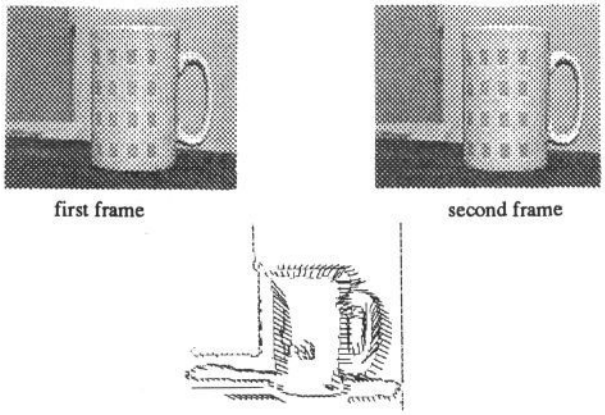

Figure 7: Results from the improved algorithm.

simply because on one hand there are lots of noises both from the original image, and from the image quantisation; and on the other hand, the computation of second order derivatives are well known to be sensitive to noise. Therefore, we consider the local tangential flow as an *approximate* local constraint for the full flow computation, as in equation 17 rather than as a precise calculation. The result from applying our improved Hildreth's method on the real image sequence is shown in figure 7. This result didn't show us a great change in the time consuming (about half the iterations as Hildreth's does). The reason can be explained as there are not enough seeds along the edges; also we don't take their tangential flow as boundary conditions which turns out that the seed's contributions are buried in or smoothed by the non-seed's normal flow. This leads to our following consideration of an alternative way for applying the c.m.c.e.

Currently, we compute a fairly good approximation to the local tangential flow at the seed loci, or we compute the tangential flow everywhere on the edge by setting the threshold of $det\mathbf{H}$ to zero, which will give us a very low confidence about the tangential flow at the loci of low $det\mathbf{H}$. Consequently, our current investigations start from finding how to build up the local tangential flow all along the edge by propagating, instead of directly using equation 14, the tangential flow at the loci of seed to the loci of low $det\mathbf{H}$. This should give us a more confident tangential flow at those loci of $det\mathbf{H}$. Although these propagated tangential flows along the edge still can only be approximate, they will have greater confidence. We are currently exploring the possibility of using wave-diffusion processing (based on the assumption that the change of tangential flow is continuous along the edge) to give us a fast propagation along the edge. This processing will again be inherently parallel. After we have the tangential flow everywhere on the edge, we combine them locally with the normal flow, to give us a very close approximation to this edgel's full flow. By this stage, we only need a few final iterations to smooth the whole flow globally to overcome the initial error that derives from *noise* rather than from *insufficient constraint*. In this way, we use the local computation as much as we can to minimise the involvement with the global computation. Therefore, most of our computation can be done in parallel. The reasons for doing this is to understand how we can propagate the reliable optic flow into less constrained regions and at the same time how much parallelism can be achieved. The ultimate point here is to understand the multiple level optic flow computation structure. To answer the questions such as how much parallelism is associated with a certain level's computation, how we can maximally apply it, and finally, how much parallelism is in the whole optic flow computation will bring us a better understanding of the parallel computation of visual motion.

Acknowledgements

I thank my supervisor, Mike Brady, for providing the initial ideas in this work, and for very helpful discussions and suggestions. Thanks to Bernard Buxton for very valuable comments both in the mathematic and in the context of the paper. Also thanks to David Murray, Guy Scott, Andrew Zissermen and all the others in Vision Lab. for help in various ways.

References

[1] J.M. Brady. Seeds of Perception. In *Proceedings of The Third Alvey Vision Conference*, pages 259–267, University of Cambridge, Cambridge, England, September 1987.

[2] L.S. Davis, Z. Wu, and Sun H. Contour Based Motion Estimation. *Computer Vision, Graphics and Image Processing*, 23:313–326, 1983.

[3] Shaogang Gong. *Parallel Computation of Visual Motion.* MSc. Report, Oxford University, England, July 1987.

[4] Haralick, R.M. Digital Step Edges from Zero-crossings of Second Directional Derivatives. *IEEE Trans. Pattern Anal. and Machine Intell.*, PAMI-6(1):58–68, 1984.

[5] E.C. Hildreth. *The Measurement of Visual Motion.* MIT Press, Cambridge, Mass., 1984.

[6] B.K.P. Horn and B.G Schunck. Determining Optical Flow. *Artifical Intelligence*, 17:185–203, 1981.

[7] Koenderink, J.J. Optic Flow. *Vision Research*, 26(1):161–180, 1986.

[8] Koenderink, J.J. and Doorn, A.J. Local Structure of Movement Parallax of the Plane. *J. Opt. Soc. Am.*, 66(7):717–723, 1976.

[9] H.H Nagel. An Investigation of Smothness Constraints for the Estimation of Displacement Vector Fields from Image Sequences. *IEEE Trans. Pattern Anal. and Machine Intell.*, PAMI-8(5):565–593, 1986.

[10] H.H Nagel. Displacement Vectors Derived from Second Order Intensity Variations in Image Sequences. *Computer Vision, Graphics and Image Processing*, 21:85–117, 1983.

[11] H.H Nagel. On the Estimation of Optical Flow: Relations between Different Approaches and Some New Results. *Artifical Intelligence*, 33:299–324, 1987.

[12] J. Alison Noble. *The Geometric Structure of Images.* MSc. Report, Oxford University, July 1987.

[13] Ramachandran, V.S. Apparent Motion of Subjective Surfaces. *Perception*, 14:127–134, 1985.

[14] Ramachandran, V.S. and Anstis, S.M. Perceptual Organization in Multistable Apparent Motion. *Perception*, 14:135–143, 1985.

[15] G.L Scott. *The Four Line Method of Locally Estimating Optical Flow.* Technical Report, University of Sussex, England, 1986.

[16] A.M. Waxman and K. Wohn. Contour Evolution, Neighbourhood Deformation and Global Image Flow: Planar Surfaces in Motion. *The International Journal of Robotics Research*, 4(3):95–108, 1985.

[17] R.J. Woodham. Analysing Images of Curved Surfaces. *Artificial Intelligence*, 17:117–140, 1981.